Water Practice & Technology

IWA PUBLISHING

Water Practice & Technology Vol 19 No 4, 1185 doi: 10.2166/wpt.2024.085

Chemically modified cellulose nanomaterial for remediation of nickel and lead from secondary runoff industrial wastewater

Hizkeal Tsade Kara [a,*], H. C. Ananda Murthy[b,c], T. Naveen Kumar[d] and C. R. Ravikumar[e]

[a] Department of Applied Chemistry, School of Applied Natural Sciences, Adama Science and Technology University, P.O. Box 1888, Adama, Ethiopia
[b] Department of Prosthodontics, Saveetha Dental College & Hospital, Saveetha Institute of Medical and Technical Science (SIMAT), Saveetha University, Chennai 600077, Tamil Nadu, India
[c] Department of Applied Sciences, Papua New Guinea University of Technology, Lae, Morobe Province, 411, Papua New Guinea
[d] Department of PG-Chemistry Surana College Autonomous, Affiliated Bangalore University, Bangalore 560004, India
[e] Research Centre, Department of Science, East West Institute of Technology, Bangalore 560091, Karnataka, India
*Corresponding author. E-mail: hizkeal.tsade@astu.edu.et

HTK, 0000-0002-6700-1978

ABSTRACT

An innovative and chemically amended succinic anhydride cellulose nanomaterial (S-CNM) adsorbent was synthesized from dried stem of *Eichhornia crassipes* weed, and was characterized for functional groups, crystallite size, surface morphology, morphological structure and particle size using Fourier transform infrared (FT-IR), X-ray diffraction (XRD), scanning electron microscopy (SEM), transmission electron microscopy (TEM) and Brunauer–Emmett–Teller (BET) instruments, respectively. Previously characterized S-CNM was investigated to eliminate nickel and lead from secondary runoff wastewater (SERWW). Physicochemical properties of SERWW including organic matter (OM), nutrients, total inorganic nitrogen (TIN) and total phosphorus (TP) on the elimination capabilities of heavy metals were investigated. The S-CNM adsorbent was used fruitfully to exclude nickel and lead from SERWW. The mechanism study showed that the Langmuir isotherm was suited for lead removal and Freundlich isotherm was suited for nickel removal with maximum eliminating capability (q_{max}) of 156.25 and 60.24 mg g^{-1} using the S-CNM adsorbent, respectively. The elimination kinetic process fits well with pseudo-second-order and its data recommending the materials (S-CNM) are effective for wastewater treatment. The lead and nickel uptake capacities were influenced by the presence of positively charged ions. The S-CNM adsorbent indicated excellent reproducibility and was considered as a capable adsorption resource to eliminate lead and nickel from SERWW.

Key words: adsorption, cellulose material, lead and nickel elimination, surface modification, wastewater

HIGHLIGHTS

- This is a novel research work because it focuses on a recent research area known as water remediation.
- The material used for remediation purposes is noble and new that is environmental friendly.
- The remediation technique was very cost-effective.
- The material used was easily recyclable.
- The material was modified by suitable chemicals that enhance the remediation processes.

GRAPHICAL ABSTRACT

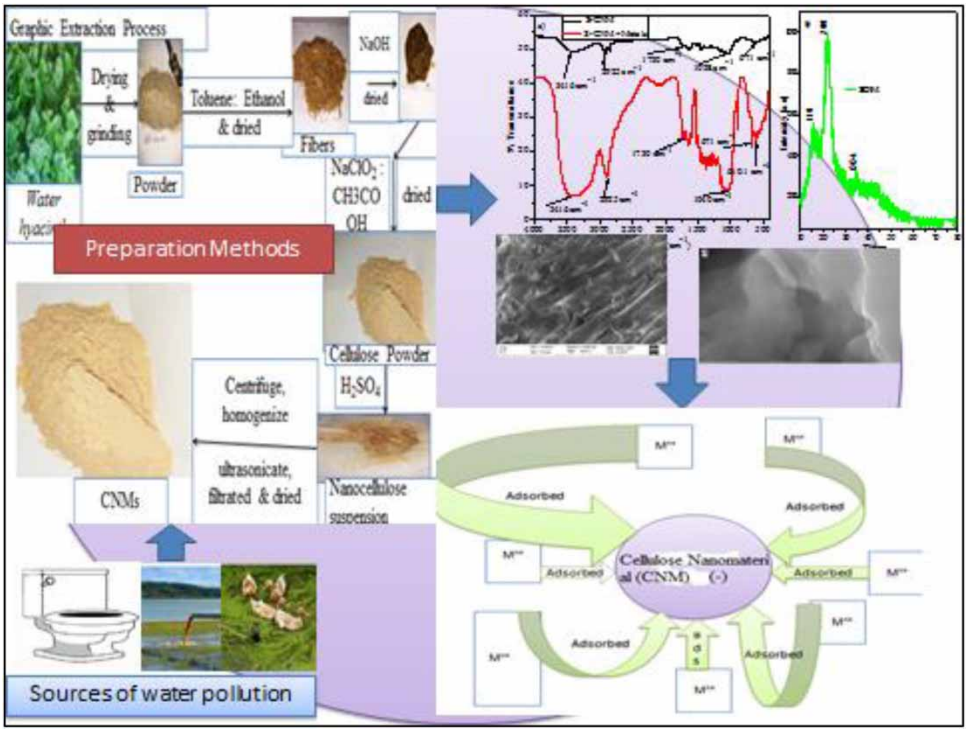

1. INTRODUCTION

Water is paramount for the sustainable development of all healthy life throughout the world (Berger *et al.* 2017; Brandes *et al.* 2019; Maharana *et al.* 2020; Shahnaz *et al.* 2020; Tsade *et al.* 2020; Tshikovhi *et al.* 2020). However, water pollution with toxic metals is recently considered the greatest stimulating issue all over the world (Anush *et al.* 2019). Nowadays, the presence of various contaminants including toxic inorganic nutrients, different organic species and fuel-related products have been reported throughout the world in aquatic systems (Briffa *et al.* 2020; Sharma *et al.* 2021; Tsade *et al.* 2021). As a result of their toxicity and bioaccumulation potential, the above-stated pollutants pose serious hazards for human beings and other environments (He *et al.* 2017; Amanda *et al.* 2020; Ibrahim *et al.* 2020). Especially, water contamination arising from toxic inorganic metals results in serious adverse impacts on the environment and human health (Bhanjana *et al.* 2017; Shahnaz *et al.* 2020; Tshikovhi *et al.* 2020). As a result of this, unlike organic contaminants, toxic inorganic nutrients are not biodegradable and can be accumulated for a long time within the tissues of living organisms, producing many illnesses and syndromes, such as cancer (Atkovska *et al.* 2018; Nguyen *et al.* 2019). Inorganic nutrients including, nickel, lead, arsenic, mercury and cadmium, to name a few, may be considered the most toxic of heavy metals in marine bodies. Increased amounts of these metals discharged into marine systems cause severe well-being and ecological risks and possibly will lead to a rise in water purification prices. For example, the toxicity of lead can affect the reproductive systems, intelligence index, and kidney and liver illnesses (Gaurav *et al.* 2017; Xu *et al.* 2017). Moreover, regarding the studies conducted in toxicological on nephrotoxicity, the introduction of lead into the human body can be related to renal tubular necrosis, and this introduction is directly related to the failure of glomeruli (Rathnasekara *et al.* 2021). Exposure to nickel, on the other hand, can harm the lungs, stomach, kidneys, and cause cancer (Ibrahim *et al.* 2020). Because of this, eliminating heavy metals, in general, and lead and nickel, in particular, from wastewater before discharging it into the environment, is of the highest interest. Traditional methods for the elimination of these types of toxic inorganic nutrients include adsorption, coagulation, precipitation, filtration, solvent extraction, reverse osmosis, and ion exchange (Matsis and Grigoropoulou 2008; Anjum *et al.* 2019; Agnes *et al.* 2020; Mohib *et al.* 2020). Nevertheless, some of these cause high operational costs, with relatively low eradication capacities and more often treated waters need an extra polishing step or steps to achieve desired removals, thus making it even more expensive (Mohd Nor *et al.* 2021). Adsorption, however, has demonstrated lower running costs, and large removal capacities and has presented itself as a plausible

alternative. Even further, the use of adsorbent materials is widespread including activated carbon, carbon nanotubes (CNTs), and nanocomposites (Alipour *et al.* 2020), making it the technology of choice (Hokkanen *et al.* 2016).

But, from these polymeric materials, cellulose has more merits such as easy to obtain, not toxic, as well as more available hydroxyl functional groups taht are accessible for different chemical amendment reactions (Jianhua *et al.* 2020; Yeit *et al.* 2020; Kara *et al.* 2021a). In spite of its pronounced merits, the demerits of cellulose in wastewater cleaning are its delayed hydrophilicity, less physical and chemical stability, and limited pollutant uptake capability (Anirudhan & Deepa 2015). Due to this reason, nowadays, the synthesis of nanomaterials for adsorbing adsorbate is growing (Ahankari *et al.* 2020). However, nanomaterials, including titania-doped nanotube, carbon-based nanotube, and zerovalent iron nanomaterials are toxic and not suitable for pollutant elimination (Ahankari *et al.* 2020). These drawbacks were easily resolved by synthesizing adsorbent materials by disintegrating cellulose materials into cellulose nanomaterials (CNMs) using different preparation methods (Kim *et al.* 2015; Kara *et al.* 2021b). Regarding its synthesis methods and origin materials, nanocellulose could be categorized into cellulose nano-fibers (CNFs), cellulose nano-crystals (CNCs), and bacterial-cellulose (BC) (Hokkanen *et al.* 2016). In this study, CNC was prepared by using the sulfuric acid hydrolysis method.

A number of investigations have been carried out previously on the nanocellulose-based adsorbent materials prepared from different natural resources such as date palm (*Phoenix dactylifera L.*) (Adel *et al.* 2018), residue from cotton (Do Nascimento *et al.* 2015), banana linters (Harini *et al.* 2018), husk obtained from corn (Yang *et al.* 2017), and others. As per the knowledge of the researcher, few works were reported using CNMs prepared from the dried stem of *Eichhornia crassipes* weed collected from Lake Abaya. Also, for the improvement of the CNM surface area, it was modified using succinic anhydride chemical in the carboxyl group. In addition to this, to the greatest of the researcher's knowledge, most of the research carried out in the reported references were using aqueous solution merely, but there is a research gap on real wastewater treatment. Therefore, this study aims at looking at the CNM prepared from dried stem of *E. crassipes* weed resources for the elimination of nickel and lead found in SERWW.

2. METHODOLOGY

2.1. Different chemicals

The analytical grade chemicals were purchased and used for all the experiments. They were namely, $NaClO_2$ (80%, Shanghai ZZ New Material Tech. Co., Ltd, China), CH_3CH_2OH (97%, Tradewell International Pvt. Ltd, India), toluene (99%, Loba Chemie Pvt. Ltd, India), NaOH (99%, Shraddha Associates (GUJ) Pvt. Ltd, India), conc. HCl (35%, Loba Chemie Pvt. Ltd, India), conc. H_2SO_4 (69%, Loba Chemie Pvt. Ltd, India), conc. HNO_3 (69%, Loba Chemie Pvt. Ltd, India), $Ni(NO_3)_2$ (99%, Shraddha Associates (GUJ) Pvt. Ltd, India), $Pb(NO_3)_2$ (99%, Shraddha Associates (GUJ) Pvt. Ltd, India), and $NaHCO_3$ (99%, Shraddha Associates (GUJ) Pvt. Ltd, India).

2.2. Sample collection and cellulose nanomaterial preparation

The stem of the weed found in the aqueous system, namely *E. crassipes* for CNM fabrication was collected randomly from Lake Abaya 'Arba Minch', Gamo Zone, Ethiopia. Next, the secondary runoff industrial wastewater (SERWW) was acquired from the Modjo area, Oromia Region, Ethiopia. After this, the randomly collected and dried stem of the *E. crassipes* weed sample was washed with distilled water many times and dried with air at room temperature and grinded with a clean mill. Then, cellulose was fabricated by taking 10 g of carefully dried stem of *E. crassipes* plus a mixture of 1:1.5 of toluene to ethanol solvent for about 48 h at 50 °C followed by cleaning with hot water and dried out in oven for 10 h at 50 °C. Then, the fabricated and dried-out fibers were adjusted into short fibers of roughly 5 mm in length. Following, the adjusted cellulose fibers were cured with 90 mL of 2.25 M NaOH solution at 60 °C for 2.5 h for the removal of lignin and hemicelluloses found in *E. crassipes* biomass. This solution was cleaned carefully with deionized water repetitively till a solution with pH of 7 was obtained. Again, the obtained solution with pH of 7 was clarified, centrifuged and dried out in the oven at 60 °C for 12 h. At this stage, the solution reached a pulp form through a careful grinding procedure and the bleaching procedure was performed with a 3.5:1.5 mixture of sodium chlorite ($NaClO_2$) and glacial acetic acid for 5 h at 70 °C through mechanical stirring. Then, the obtained residue solution was constantly centrifuged, clarified and dried out to get the suspension of cellulose. The suspension of cellulose was cleaned from any impurities such as lignin, hemicellulose, fluid by careful treatment with 90 mL of 2.25 M NaOH solution. In order to obtain

cellulose-free from any non-cellulose components, this procedure was reiterated by half of the initial amount of bleaching reagent. Following this, the solution was hydrolyzed using 90 mL of 6.5 M H_2SO_4 for 3 h to carefully break down the cell wall into smaller fibers and to isolate the fibrils from each other. At this stage, the white suspension of CNM was centrifuged at 12,000 rpm to separate the CNM and homogenized in a homogenizer at about 12,000 rpm for 3 h. Finally, the fabricated CNM was stored in an appropriate place and analyzed for characterization of different required techniques. These experimental steps were taken by Kara *et al.* (2021a, 2021b) through slight modification.

2.2.1. Preparation of chemically amended CNM

For the fabricated CNM surface amendment, 20 g of CNM suspension was taken and treated with 0.19 L of NaOH solution (19 wt.%) at 25 °C for 17 h through magnetic stirring. After this, the basic-CNM obtained was isolated from the mixture solution through the centrifuge and cleaned with deionized water until the solution got pH of 7, clarified and dried out. Then, 10 g of the isolated CNM was treated with 20 g of succinic anhydride for 18 h. This chemically amended CNM suspension was centrifuged and clarified, cleaned by using dimethylformamide (DMF), ethanol 95%, distilled water, HNO_3 (0.01 mol/L), and acetone sequentially. Finally, the carefully cleaned chemically amended CNM was reacted with a saturated sodium bicarbonate solution for 45 min through fixed stirring and afterwards filtered,and finally cleaned with the help of deionized water and then acetone and dried out at room temperature to produce S-CNM. This experimental step was adapted from a study reported by Hokkanen *et al.* (2016) with a minor amendment. Afterwards, the chemically amended CNM was stored in a suitable place until the end of the experimental work. The modification chemical reaction is given in Figure 1.

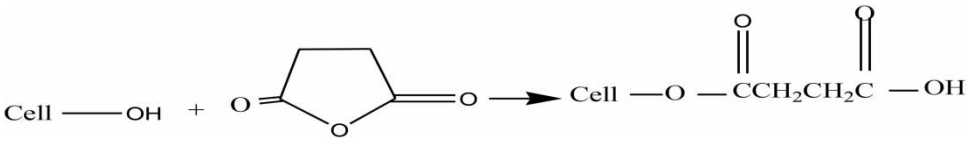

Figure 1 | Modification reaction of cellulose nanoparticles with succinic anhydride.

2.3. Characterization

The crystallite size of the S-CNM adsorbent was analyzed with the help of an XRD instrument (Cu-Kα radiation ($\lambda = 0.154$ nm) at 40 kV and 40 mA under a 2θ diffraction angle from 0° to 40° at a scan rate of 2°/min). The functional group found on the fabricated S-CNM adsorbent was recognized through the help of FT-IR (Perkin-Elmer, RXI model). The morphology characteristic of the fabricated S-CNM adsorbent surface was observed using a Hitachi S-4100 scanning electron microscope (SEM). The specific surface area (SSA) determination was performed by Brunauer–Emmett–Teller (BET) analysis. The particle size of the S-CNM adsorbents was determined using a transmission electron microscope (TEM).

2.4. Adsorption experiments

First, the 1,000-ppm stock solution of nickel and lead ions was prepared from their soluble salts and the stock solution with the necessary amount of the synthesized and characterized adsorbent (S-CNM) dose was mixed in a 100-mL flask by diluting to the required adsorbate concentrations and stirred with an orbital for 150 min. The solution pH of nickel and lead was justified with the help of dilute HCl and NaOH solutions through pH meter. The use of one separation technique, namely filtration separates the solid/liquid phases of the solution. After this, the absorbance measurement of nickel and lead ions was performed with the help of a flame atomic absorption spectrophotometer (FAAS, Shimadzu, USA). The above all experiments were performed by measuring different constituents that affect the removal capability of nickel and lead ions, including, contact time ranging from 20 to 180 min, solution pH ranged from 2 to 10, adsorbent dose ranged from 0.02 to 3.0 g, and initial adsorbate concentration ranged from 5 to 40 mg/L. The influences of every component on the removal capability of nickel and lead ions were performed by putting the rest components at a constant system.

2.4.1. Adsorption isotherms

Isotherms performed for the uptake of nickel and lead metals by the adsorbent (S-CNM) are the most imperative scientific exemplary to explain the process of adsorption of metal ions on the solid and liquid phases of the sorbent based on a set of images related to the kind of occupancy, how heterogeneous or homogeneous the solid

S-CNM surface and the chance of interaction between nickel and lead ions. Thus, the quantity of nickel and lead ions removal by adsorption was anticipated through the use of a mass balance on the adsorption method. This method indicates that the amount of nickel and lead metal ions uptake by the S-CNM adsorbent is proportional to the amount of Ni(II) and Pb(II) ions that were removed from the SERWW. The illustration of the process can be accessible in the following equations:

$$q_e = \frac{C_i\text{Ni(II)\& Pb(II)} - C_e\text{Ni(II)\& Pb(II)}}{\text{S}} \tag{1}$$

$$q_t = \frac{C_i\text{Ni(II)\& Pb(II)} - C_t\text{Ni(II)\& Pb(II)}}{\text{S}} \tag{2}$$

Here, q_e and q_t characterize the quantity of nickel and lead ions adhered on the adsorbent (S-CNM) apparent at optimum (equilibrium) and at a specified period of time (mgg^{-1}), respectively. C_iNi(II) and Pb(II) ions and C_e Ni(II) and Pb(II) ions represent the initial and equilibrium levels of the Ni(II) and Pb(II) ions in the SERWW sample (mgL^{-1}), respectively and C_t is the levels of Ni(II) and Pb(II) ions in SERWW sample (mgL^{-1}) at a specific time. S indicates the suspension dose that gives information on the S-CNM adsorbent mass (g) to the initial volume of water sample (L) ratio. Concentrations that were calculated initially and calculated at equilibrium describe the percentage removal of Ni(II) and Pb(II) ions (Equation (3)).

$$\%\text{Heavy metal removal} = \frac{C_i\text{Ni(II)\& Pb(II)} - C_e\text{Ni(II)\& Pb(II)}}{C_i\text{Ni(II)\& Pb(II)}} \times 100\% \tag{3}$$

2.4.2. Adsorption kinetics

The rate of adsorption mostly depends on the contact time and is termed the most significant parameter providing valuable data for the velocity of sorption. It also evaluates the Ni(II) and Pb(II) ions uptake capacity of S-CNM adsorbent from SERWW. Thus, the adsorption kinetics mechanism of Ni(II) and Pb(II) ions from SERWW was studied at a contact time of 20–180 min and maintaining constituents (pH of the solution, S-CNM dose, and Pb(II) and Ni(II) ions starting levels) at optimum.

2.5. Regeneration experiment

The reusability study of the previously used S-CNM adsorbent in the adsorption of nickel and lead ions in the SERWW was done by duplicating the experimental procedures through the use of similar S-CNM adsorbent for four consecutive circles. Desorption of nickel and lead ions was performed through the addition of the optimum S-CNM value (0.3 g) previously used for eradicating nickel and lead ions from SERWW in a conical flask with 10.5 mL of 0.1 M HCl solution for 19.5 min and sonication for 6 min was performed. Afterwards, the material (S-CNM) was easily alienated from the mixture by centrifugation. The alienated material (S-CNM) was washed away with the help of distilled water six times, dried out and reapplied for four consecutive cycles.

3. RESULTS AND DISCUSSION

3.1. Characterization

The chemically amended cellulose nanoparticle (CNP) adsorbent was analyzed through the help of FT-IR, XRD, SEM BET, and TEM modern instrumental techniques. A powerful tool named FT-IR spectroscopy was used to identify the presence of different functional groups available for the fabricated S-CNP adsorbent as well as its spectra before and after adsorption is displayed (Figure 2(a)). The peaks indicated at 3,416 cm^{-1}, 2,853–2,925 cm^{-1}, 1,730 cm^{-1} and 1,058 cm^{-1}, before and after adsorption confirm the presence of O-H stretching, C-H stretching, C-O stretching, and C-O-C stretching vibration of cellulose-I, respectively (Kara *et al.* 2020; Haoyuan *et al.* 2023). The wide peak and the strident peak before and after adsorption, respectively, at 671 cm^{-1} resemble ß-glycosidic associations between cellulose glucose units. The occurrence of this peak in this study is stimulating meanwhile it is a suggestion that the acid hydrolysis process may have not lost the cellulosic material nature. The extra peak at 610 cm^{-1} showed that there is a chemical reaction occurring between S-CNP and metal ions. This is a confirmation of the adsorption of nickel and lead ions on the surface of the S-CNP adsorbent (Kara *et al.* 2020). In conclusion, S-CNP adsorbent contains abundant carboxyl, hydroxyl, and ester

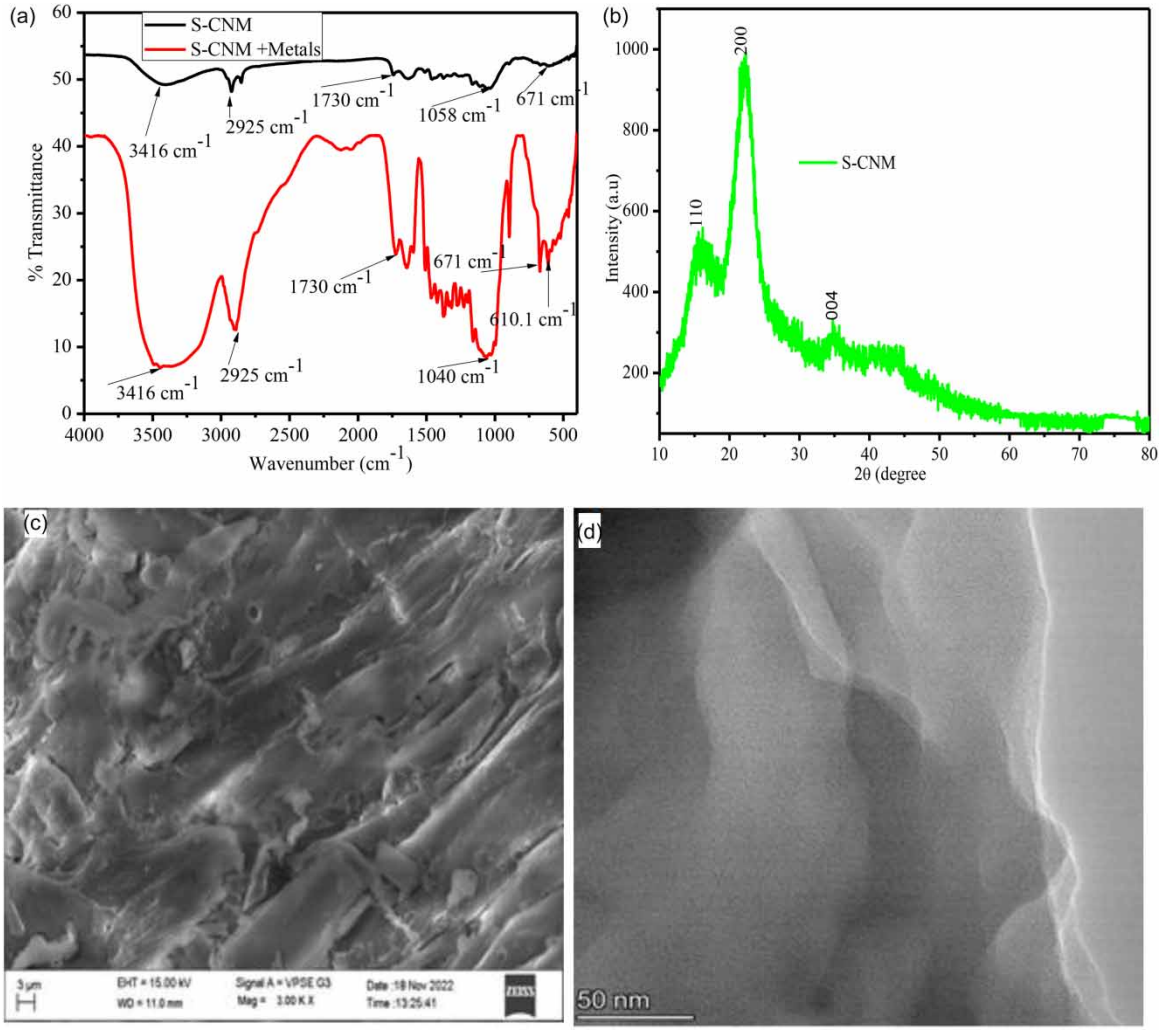

Figure 2 | (a) FT-IR spectral images of the S-CNP adsorbent, (b) XRD spectra of of the S-CNP adsorbent, (c) SEM images of the of the S-CNP adsorbent, and (d) TEM images, of the S-CNP adsorbent, respectively.

functional groups that have large vacant spaces to adsorb nickel and lead ions by electrostatic interaction between the negatively charged S-CNP adsorbent and positively charged nickel and lead ions (Kara *et al.* 2020).

Figure 2(b) displayed the X-ray diffractometer spectra of the synthesized CNP to govern the crystallinity size. As shown, the spectral main peaks at 15.99°, 22.22° and 34.97° indicate the respective cellulose-I structure and correspond to the crystals of the representative plane description of 110, 200, and 004, respectively (Anirudhan & Deepa 2015; Kara *et al.* 2020). The S-CNP adsorbent crystallite size was calculated and the value was 2.45 nm. Likewise, its width was 3.65 nm. Similar to this, Anirudhan & Deepa (2015) reported similar results that entitled on correlating nanocrystalline cellulose particle size and its surface area. Generally as seen from the peaks, a semi-crystalline with unstructured broadened hemp and crystalline peaks was observed. This is owing to the circumstance that the S-CNP was fabricated from natural-based materials, which could not show a 100% crystallinity environment. Additionally, the esterification process of the cellulose was achieved with the reaction of succinic anhydride to form an esterified cellulose nanoparticle (S-CNP). The semi-crystallinity structure of CNM was confirmed by XRD analysis (Kara *et al.* 2020).

Figure 2(c) and 2(d) depicts the morphology of S-CNP adsorbent. As shown in the figure, a rod-shaped spectral peak, which exhibited an organized and importantly penetrable cooperated assembly with indelicately even pore sizes with augmented definite surface areas, was detected. This consequently resulted due to the extreme homogenization of the adsorbent constituents throughout fabrication development and this meaningfully increased the surface area to volume ratio for S-CNP adsorbent. Additionally, the fibers of S-CNP are particularly disconnected from each other. The succinic anhydride modification process showed the actual rough surface S-CNP adsorbent detected by SEM micrographs. As a result, the surface area of S-CNP is augmented through the

S-CNP adsorbent roughness of the surface and reducing the particle size (Zhou *et al.* 2012). Therefore, excess vacant sites exist for nickel and lead metal ions adsorption. The morphological feature of S-CNM was measured by TEM interpretations (Figure 2(d)). The image shows the nanosized fibril with a wide heterogeneous distribution both in width and in length.

Data analysis of BET conferring to its linear equation given in Equation (4) for description of the S-CNP adsorbent SSA is done. This determination was performed at a temperature of 77 K through the use of adsorbate termed N_2 gas.

$$\frac{p/p_o}{n(1-p/p_o)} = \frac{C-1}{(X_m C)}(p/p_o) + \frac{1}{X_m C} \tag{4}$$

In the above equation, P_o and P represent saturated and partial vapor pressure of N_2 gas at equilibrium in pa, respectively; n represents the N_2 gas volume adsorbed at STP by using mL as a unit; X_m represents BET monolayer capability; C represents a dimensionless constant associated with the enthalpy of N_2 gas adsorption on the adsorbent.

Nanoparticles with a C value $\geq$80 were considered as a respectable BET monolayer capability (Thommes *et al.* 2015). As seen from the findings, the S-CNP adsorbent value for C is 190.6 indicating that the value showed a respectable BET monolayer capability. After this, the linear plots of $[(P/P_o)/(n(1-P/P_o))]$ versus P/P_o are indicated in Figure 3(a), showing a straight line with estimated comparative value for pressure presented in the range between 0.05 and 0.3. The regression result (0.9982), which is greater than 0.995 indicated the confirmation of the satisfactory level of regression value. Based on the following equation, the SSA in $m^2 \cdot g^{-1}$ value is obtained.

$$a_s = \frac{X_m L \sigma_m}{mx22400} \tag{5}$$

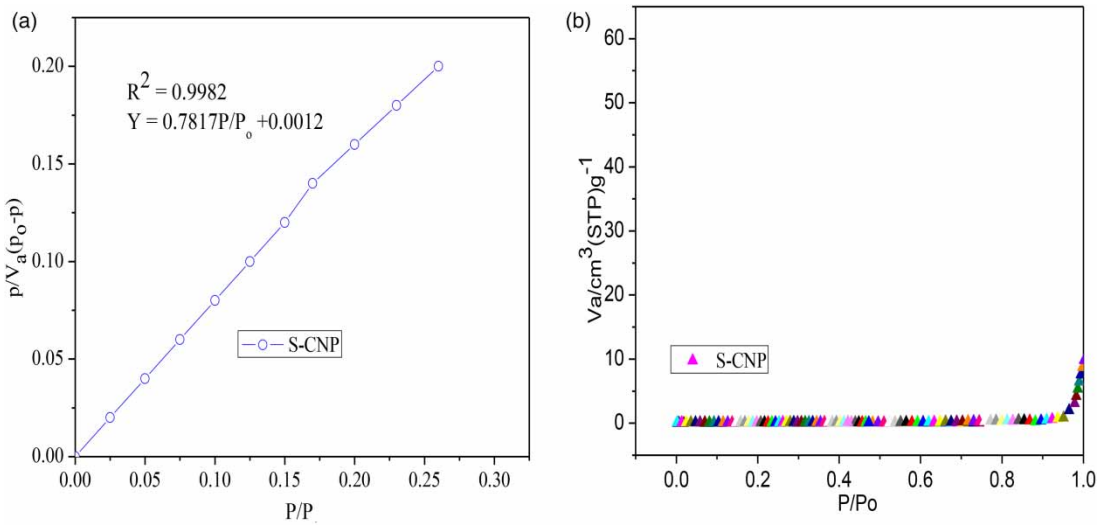

Figure 3 | (a) The S-CNP linear plot and (b) the S-CNP BET plot.

In the above equation, L represents Avogadro constant (6.022×10^{23} mol^{-1}), a_s represents the S-CNM adsorbent SSA of the mass m in grams for BET analysis, σ_m represents N_2 gas molecular adsorptive cross-sectional area in the complete monolayer (equal to 0.162 nm^2 for N_2 gas) analysis, the 22,400 represents the amount of occupied volume in mL by 1 mole of N_2 gas at STP. The cylindrical shape of the S-CNP adsorbent was observed from the BET plot given in Figure 3(b). Findings showed that the synthesized S-CNP adsorbent has a higher SSA of 124.82 $m^2 g^{-1}$. Therefore, S-CNP adsorbent has shown higher metal adsorption competence owing to the decline and increase of S-CNP adsorbent particle size and SSA, respectively, observed from BET data analysis.

3.2. Physicochemical properties of the SERWW

The collected SERWW physicochemical analysis values are presented in Table 1. As seen in Table 1, the pH average value was 5.7 ± 0.04. From the pH result, nearly acidic SERWW was collected from the Modjo River. Subsequently, the SERWW average values for COD and BOD were 70.9 ± 0.03 and 65.04 ± 0.02 mg/L, respectively. Following this, the SERWW average values for Fe^{2+}, TDS, Cl^-, SO_4^{2-}, Ca^{2+}, Mg^{2+}, and Cu^{2+}

Table 1 | Physicochemical analysis study of the SERWW

Parameter in mg/L, except pH	Average values
pH	5.7 ± 0.04
COD	70.9 ± 0.03
BOD	65.04 ± 0.02
Iron	0.59 ± 0.03
TDS	40.4 ± 0.02
Cl^-	39.3 ± 0.02
Ca^{2+}	90.5 ± 0.05
Mg^{2+}	89.6 ± 0.02
Cu^{2+}	0.50 ± 0.03

COD, chemical oxygen demand; BOD, biochemical oxygen demand; TDS, total dissolved solid.

were 0.59 ± 0.05, 40.4 ± 0.02, 39.3 ± 0.02, 90.5 ± 0.05, 89.6 ± 0.2 and 0.50 ± 0.02 mg/L, respectively. As seen from the result, cations and anions are present in the collected SERWW and reacts with the Ni(II) and Pb(II) ions in the adsorption mechanisms.

3.3. Adsorption experiments

3.3.1. Effect of interaction periods of time

The effects of interaction periods of time on the adsorption of Ni(II) and Pb(II) ions in the SERWW were accompanied by changing the interaction periods of time from 30 to 180 min at an optimum dosage of 0.5 g for S-CNP, 25 °C of temperature (T), and initial concentration of Ni(II) and Pb(II) ions of 30 mg L^{-1} (Figure 4(b)). The greater adsorption processes were perceived by increasing the interaction periods of time ranging from 30 to 180 min for S-CNP adsorbent. This is due to the availability of a large number of vacant spaces in the S-CNP adsorbent (Sun *et al.* 2018; Kara *et al.* 2020). The S-CNP adsorbent maximum percentage removal (%R) of Ni(II) and Pb(II) ions were 84 and 95.0%, respectively, and was perceived at the optimum periods of time equal to 120 min for Ni(II) and Pb(II) ions, respctively. Beyond this, the metal uptake process attempts the equilibrium position and process in a fixed manner. This result agrees with research reported by Unuabonah *et al.* (2007), on lead(II) ions adsorbed onto phosphate-modified kaolinite clay adsorbent.

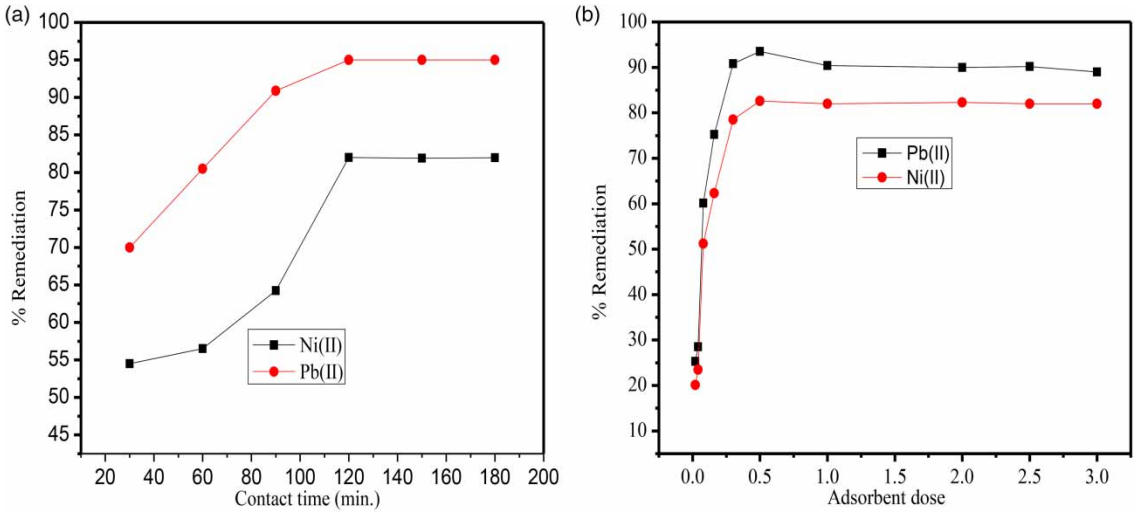

Figure 4 | Effect of interaction periods of time (a) and S-CNP adsorbent dose (b) for the removal of nickel and lead ions from SERWW, correspondingly, at optimum (temperature of 25 °C, metal initial concentration of 30 mg/L, and solution pH of 5).

3.3.2. Effect of adsorbent doses

As seen in Figure 4(a), the effects of S-CNP dosage on the (%R) of nickel and lead metal ions from the SERWW showed that 82.6 and 93.5% of nickel and lead metal ions, respectively, can be eliminated from SERWW through

the use of S-CNP adsorbent with an optimum adsorbent dosage of 0.5 g at room temperature. The relatively greater %R for lead ions was observed through the use of S-CNP adsorbent may be because of the solubility nature of the metals. The more soluble the adsorbate the less adsorbed onto the adsorbent. In conclusion, it can be seen that for nanosorbent the %R of both metal ions increases through the increase of the S-CNP adsorbent dose up to the optimum values. After the optimum S-CNP adsorbent, the adsorption competence declined. This is predicted as a result of the fact that at increased concentration levels of nanosorbent (S-CNP), large number of vacant spaces are available for the metal ions. However, at augmented concentration levels, there is no additional augmentation in the adsorption mechanism because of the amount of nickel and lead ions bonded to the S-CNP adsorbent and the number of movable ions in the SERWW turns into constant even with extra accumulation of the S-CNP adsorbent dose (Tana *et al.* 2018; Igberase *et al.* 2019).

3.3.3. Effect of solution pH and initial concentration

Figure 5(a) shows the influences of solution pH and initial concentration of nickel and lead metal ions on the %R of nickel and lead metal ions in the SERWW through the use of S-CNP adsorbent. S-CNP adsorbent showed increasing adsorption capabilities in the range of solution pH between 2 and 5. Correspondingly, the higher %R competence of S-CNP adsorbent was 94.5 at pH equal to 5. At acidic pH, the reaction of Ni(II) and Pb(II) ions with S-CNP adsorbent is diminished because of the interference of H^+ ions to the S-CNP adsorbent surfaces. Conversely, as the SERWW pH approaches to neutral level, nickel and lead ions adsorption to the S-CNP adsorbent surface increases. Beyond this point, an increase in pH value was recorded because of the increased concentration of OH^- ions and as a result the reduced %R of nickel and lead metal ions observed. Supporting this result, Tsade *et al.* (2021) reported a higher %R of lead metal ions at closely comparable values of pH. Additionally, on the basis of this result, Ben-Ali *et al.* (2017) reported the higher %R of copper at closely comparable values of pH. At basic pH values, the nickel and lead metal ions were precipitated as their hydroxides.

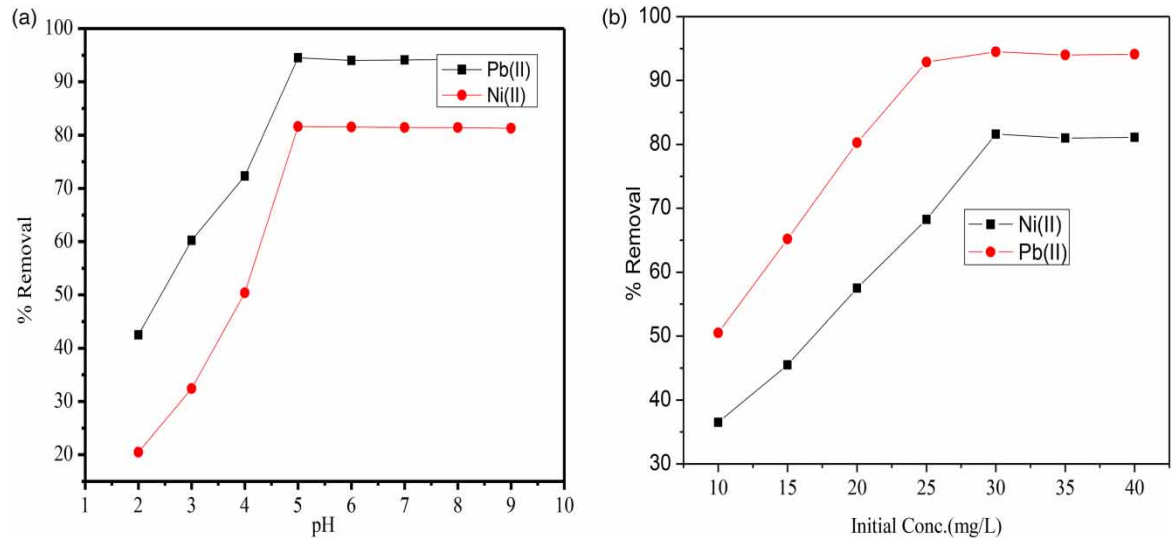

Figure 5 | Effect of solution pH (a) and initial concentration (b) for the removal of Ni(II) and Pb(II) ions from SERWW, respectively, at optimum (temperature of 25 °C, adsorbent dose of 0.5 g, and interaction periods of time equal to 120 min.).

Effects of initial concentration (C_i) of nickel and lead metal ions on the adsorption mechanism by S-CNP adsorbent is represented in Figure 5(b). At the starting point, the adsorption reaction goes as fast as and in a very short period of time it attains the equilibrium value of 30 mgL^{-1}. The quicker metal uptake processes at the starting point were a result of the large unoccupied spaces of the S-CNP adsorbent surface. At this stage, the S-CNP adsorbent clearly displayed higher uptake competence of nickel and lead metal ions. This happens as a result of the comparatively augmented SSA of S-CNP adsorbent which was observed by the reaction of CNP with carboxyl and ester-yielding chemicals (Gopal Reddi *et al.* 2017).

3.4. Effect of wastewater on the removal of nickel and lead ions

Figure 6 shows the %R of the nickel and lead ions in both aqueous solution and SERWW containing these metal ions. As seen in Figure 6, the adsorption mechanism showed a negative effect resulting from the presence of positively charged ions in SERWW. This results in the declined %R of Ni(II) and Pb(II) ions from the SERWW than the aqueous solution because of the side interaction of positively charged ions for the active sites of S-CNP adsorbent in the SERWW. As a result of this, the decrease in interaction of active sites on S-CNP adsorbent and Ni(II) and Pb(II) ions was observed and results in decreased %R of Ni(II) and Pb(II) ions. The findings were justified by the %R which were found to be 99.6 and 94.5% for the aqueous solution and real SERWW, respectively for Pb(II) ions and 99.5 and 81.5% for the aqueous solution and real SERWW, respectively for Ni(II) ions.

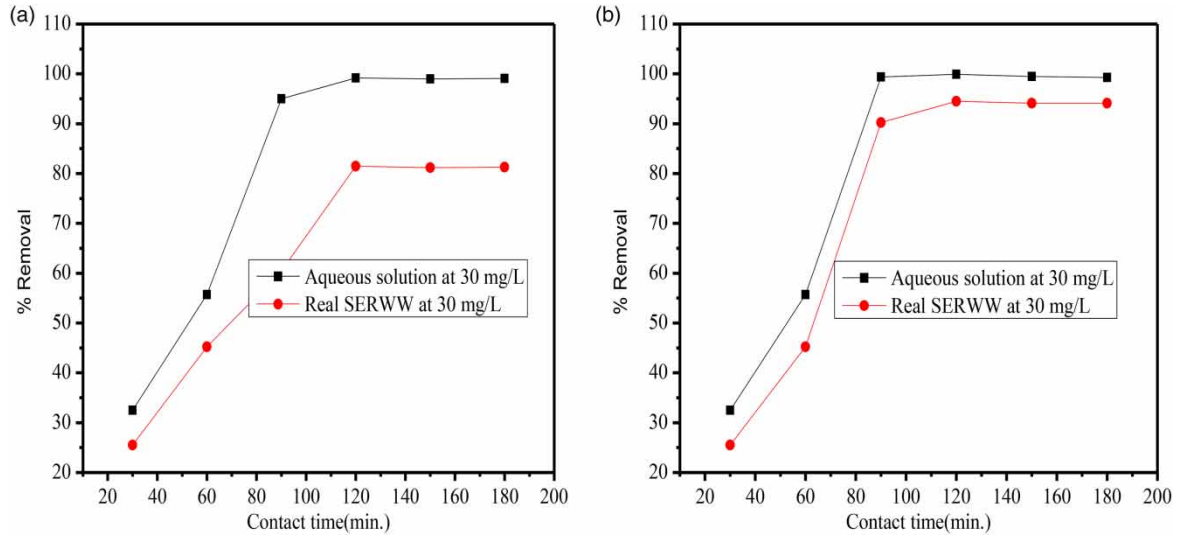

Figure 6 | The effects of wastewater chemistry (both aqueous and real SERWW, respectively) on the percent removal of Ni(II) and Pb(II) ions at optimum initial concentration equal to 30 mg/L, interaction periods of time equal to 120 min, room temperature, and adsorbent dosage equal to 0.5 g, respectively, by using S-CNP.

3.5. Adsorption isotherms

The adsorption mechanisms fit well with the Langmuir isotherm model for the removal of lead metal ions and the Freundlich isotherm model for the removal of nickel metal ions is given in Figures 7(a) and 7(b). Obviously, these isotherm models explain the distribution of nickel and lead metals among the fluid and crystalline states according to expectations related to the varied or unvaried situations of the S-CNP spaces, the assembly of exposure, and the panorama of interaction. Linear equations of the Langmuir isotherm and Freundlich isotherm were exemplified in (Equations (5) and (6)), respectively. Moreover, the value for a dimensionless equilibrium parameter (K_L) is measured through the use of Equation (7) for the confirmation of feasibility for the adsorption of Ni(II) and Pb(II) ions on S-CNP sorbent. Table 2 indicates the measured Langmuir and Freundlich isotherm constituent values. As seen in Table 2, the regression values for the Langmuir and Freundlich isotherm model through the use of S-CNP sorbent were 0.962 and 0.980, respectively, for Ni(II) removal and the regression values for Langmuir and Freundlich isotherm model through the use of S-CNP sorbent were 0.984 and 0.945, respectively, for Pb(II) removal. Furthermore, the measured amounts of the Langmuir constant b of S-CNP sorbent for Ni(II) and Pb(II) ions uptake were 0.590 and 0.030 Lmg^{-1}, respectively. In conclusion, it recommends the opportunity of adsorption mechanisms. Additionally, the quantity of K_F and n of S-CNP adsorbent for nickel and lead metal ions adsorption was (1.032 and 1.033) and (6.30 and 7.76), respectively. From the findings, one can conclude that the adsorption capability of nickel and lead metal ions as well as intensity improved, respectively. The higher nickel and lead metal ions adsorption efficiency ($q_{\max}$) of the S-CNP adsorbents in the given unit mass was 60.22 and 156.23 mgg^{-1}, correspondingly. The results showed that the S-CNP adsorbent used has a high pollutant removal capacity, in general, and a high removal efficiency

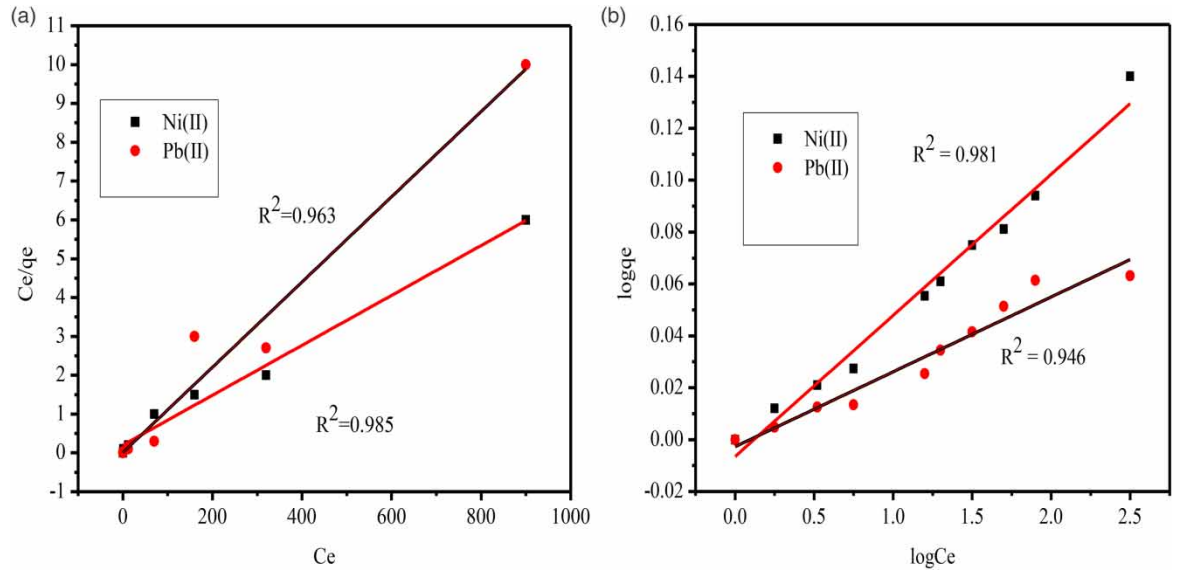

Figure 7 | Langmuir (a) and Freundlich (b) adsorption isotherms for the elimination of Ni(II) and Pb(II) ions, respectively, at a contact time = 120 min, adsorbent dose = 0.5 g, solution pH = 5, and C_i = 30 mg/L.

Table 2 | Langmuir and Freundlich isotherm model constants for nickel and lead metal ions adsorption by S-CNM adsorbent at 25 °C

	Langmuir isotherm models				Freundlich isotherm models		
Hevy metals	q_{max} (mgg^{-1})	b	K_L	R^2	K_F	n	R^2
Ni(II)	60.22	0.590	0.027	0.962	1.032	6.30	0.980
Pb(II)	156.23	0.030	0.167	0.984	1.033	7.76	0.945

of nickel and lead metal ions, in particular.

$$\frac{C_e}{Q_e} = \frac{1}{bQ_{\max}} + \frac{C_e}{Q_{\max}} \tag{6}$$

$$logqe = \log K_F + \frac{1}{n}\log Ce \tag{7}$$

$$K_L = \frac{1}{1 + bC_0} \tag{7}$$

3.6. Rate of adsorption

The rates of nickel and lead metal ions adsorption by S-CNP adsorbent were performed through the use of linear pseudo-first order (PFO) (Equation (7)) and linear pseudo-second-order (PSO) (Equation (8)), correspondingly. The plots were plotted through C_e vs. C_e/q_e and log q_e versus log C_e plot was given in Figure 8(a) and 8(b), correspondingly.

$$\log(q_e - q_t) = \log q_e - \frac{k_1 t}{2.303} \tag{8}$$

$$\frac{t}{q_t} = \frac{1}{k_2 q_e^2} + \frac{t}{q_e} \tag{9}$$

The regression investigational data found through the use of PFO kinetics model was invalid for the adsorption process due to the investigational q_e number being much dissimilar than the measured q_e value for S-CNP adsorbent. The findings specified that the rate of adsorption mechanism did not fit PFO kinetics. Thus, Figures 8(a) and

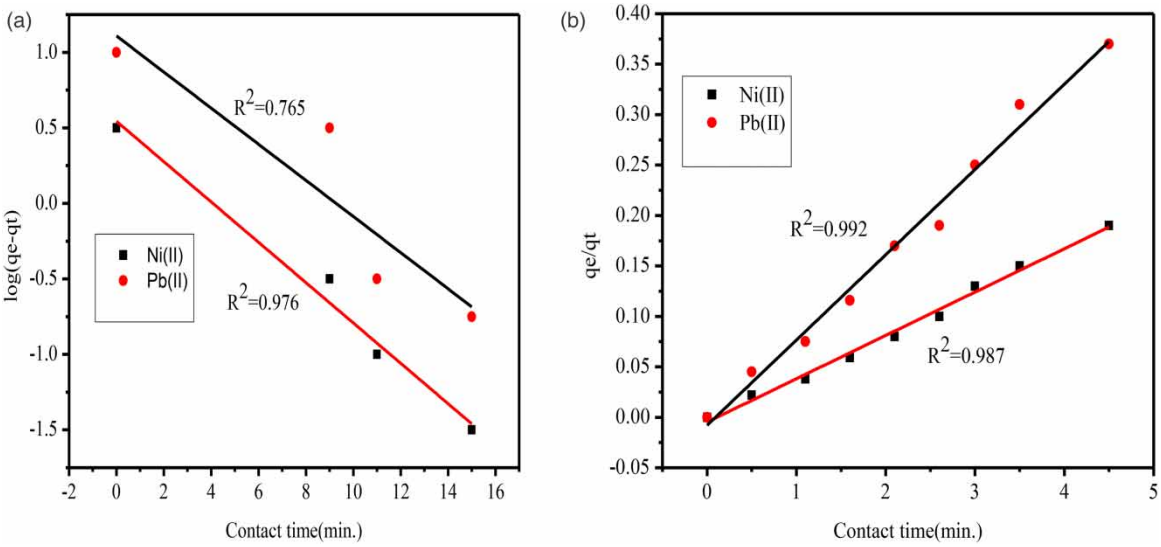

Figure 8 | Plot of the PFO (a) and PSO (b) for the elimination of nickel and lead metal ions, respectively, at interaction periods of time = 120 min., adsorbent dose = 0.5 g, solution pH = 5, and C_i = 30 mg/L.

8(b) show a PSO kinetics model that fits the study data well for nickel and lead metal ions adsorption on S-CNP sorbent. In line with this, similar research was reported by Tsade *et al.* (2021) on the adsorption of lead metal ions from wastewater through the use of CNMs. The kinetic data were found in Figures 8(a) and 8(b) and given in Table 3. The kinetics study provides a higher regression value ($R^2 = 0.985$ and 0.991, for PSO) and below satisfactory correlation coefficient value ($R^2 = 0.764$ and 0.972, for PFO) in S-CNP adsorbent for the removal of nickel and lead metal ions, correspondingly.

Table 3 | The values of parameters and correlation coefficients of pseudo-first-order (PFO) and pseudo-second order (PSO) kinetics

Kinetics	Parameters							
	PFO				PSO			
Adsorbents	q_e cal.(mg/g)	$q_{e.}$ exp.(mg/g)	k_1	R^2	$q_{e.}$ cal.(mg/g)	$q_{e.}$ exp.(mg/g)	k_2	R^2
Ni(II)	31.09	8.25	0.534	0.764	11.83	11.78	0.898	0.991
Pb(II)	5.69	5.54	0.273	0.972	23.23	23.20	0.387	0.985

3.7. Regeneration

S-CNP adsorbent regeneration investigation was accomplished to authenticate the reusability of the S-CNP adsorbent for practical application in actual schemes as given in Figure 9. This experiment was done first by desorbing the nickel and lead metal ions from the S-CNP adsorbent with the help of HCl desorption eluent through batch experiment. From the experiment, the findings show that the uptake competence of nickel and lead metal ions by S-CNP adsorbent gradually reduces with increasing rounds of recyclable experimental. The reduction in uptake competence of the S-CNP adsorbent with augmented recyclable periods of time is customarily owing to the decrease of SSA found for the S-CNP adsorbent. Satisfied recyclability by increasing nickel and lead metal ions uptake competence for the used sorbent postulates the operative sorbent of S-CNP sorbent for manipulating the uptake of contaminants. From this, one can easily understand that the adsorption competency of the S-CNP sorbent does not meaningfully alter afterwards fifth round of the experiment as the %R is still high. Results indicated that the reduction in %R for the five uninterrupted rounds was not more than 5%. From this point of view, one can conclude that the S-CNP adsorbent can be used as contaminant removal for an extended time with an increasing opportunity. This conclusion is in line with research conducted by Kara *et al.* (2021a, 2021b) for the uptake of cadmium metal ions from actual wastewater through the use of CNM adsorbent.

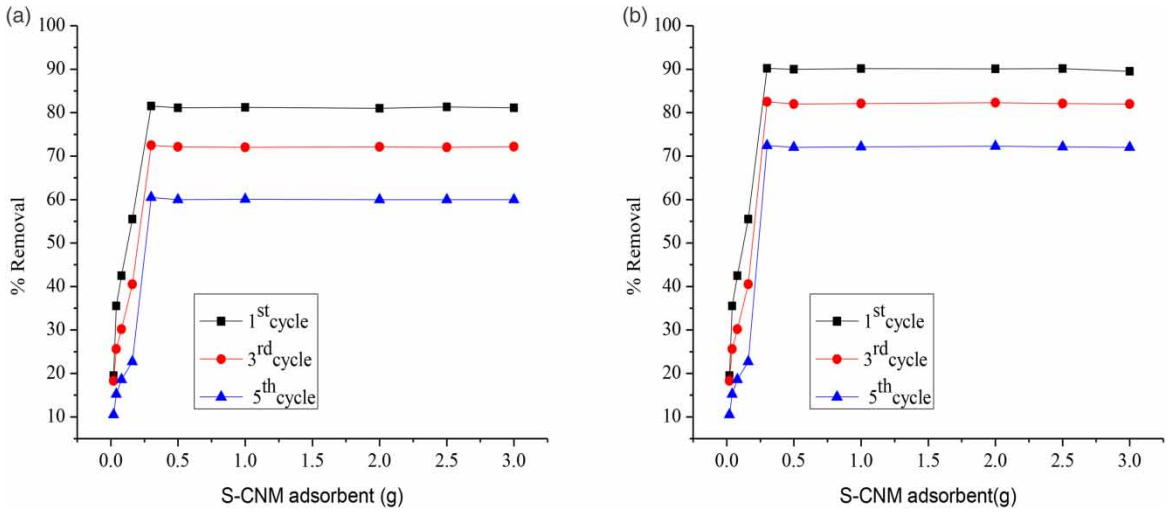

Figure 9 | Percentage of nickel and lead metal ions removals after five rounds (first, third and fifth) at C_i equal to 2 mg/L, pH equal to 5, adsorbent dose equal to 0.3 g, and interaction periods of time equal to 120 min by S-CNP sorbent.

4. CONCLUSION

Contamination by nickel and lead metal ions in an aqueous system is great owing to an enormous quantity of crude discharge of industrial wastewater from different industrial sites. As a result, the health of aqueous habitats is affected time by time. Thus, this study makes a solution to remove these contaminants before discharging them into an aqueous system. Therefore, the synthesized S-CNP adsorbent makes use of low-cost, renewable, and high uptake capability for the adsorption of nickel and lead metal ions from SERWW. The results showed that the removal capability of S-CNP toward lead metal ions in comparison with nickel metal ions was surprisingly increased due to the solubility nature of lead metal ions. From the adsorption mechanism, the lead metal ion adsorption fits the Langmuir isotherm and the nickel metal ion adsorption fits the Freundlich isotherm model. Furthermore, both metal ion adsorption fits by the PSO kinetics model. Finally, from the regeneration study, it is possible to conclude that S-CNP is an efficient adsorbent for the removal of heavy metals. Thus, from the adsorption mechanism point of view, reader can have a clue about the S-CNP adsorbent adsorption process, its characteristics, and its efficiency. Generally, as seen from the results, the synthesized S-CNP adsorbent was very efficient in removing heavy metal ions, in general, and nickel and lead metal ions, in particular.

ACKNOWLEDGEMENTS

The researcher of this study thanks Adama Science and Technology University for providing the funds and accommodation to perform this research. This research has been sponsored by the Project (ASTU, SoANS/JV-259298/2019), Research and Technology Transfer Office, Adama Science and Technology University.

DATA AVAILABILITY STATEMENT

All relevant data are included in the paper or its Supplementary Information.

CONFLICT OF INTEREST

The authors declare there is no conflict.

REFERENCES

Adel, A., El-Shafei, A., Ibrahim, A. & Al-Shemy, M. 2018 Extraction of oxidized nanocellulose from date palm (Phoenix Dactylifera L.) sheath fibers: Influence of CI and CII polymorphs on the properties of chitosan/bionanocomposite films. *Industrial Crops and Products* **124**, 155–165.

Agnes, P., Eliazer, B. N. & Augustine, E. O. 2020 Batch and continuous flow studies of Cr(VI) adsorption from synthetic and real wastewater by magnetic pine cone composite. *Chemical Engineering Research and Design* **153**, 806–818.

Ahankari, S., George, T., Subhedar, A. & Kar, K. K. 2020 Nanocellulose as a sustainable material for water purification. *SPE Polymers* **1**, 69–80.

Alipour, A., Zarinabadi, S., Azimi, A. & Mirzaei, M. 2020 Adsorptive removal of Pb (II) ions from aqueous solutions by thiourea- functionalized magnetic ZnO/nanocellulose composite : Optimization by response surface methodology (RSM). *International Journal of Biological Macromolecules* **151**, 124–135.

Amanda, A., Rifathin, A., Arum, A. & Sampora, Y. 2020 Oil palm empty fruit bunch-based nanocellulose as a super-adsorbent for water remediation. *Carbohydrate Polymer* **229**, 115433.

Anirudhan, T. S. & Deepa, J. R. 2015 Synthesis and characterization of multi-carboxyl-functionalized nanocellulose/nanobentonite composite for the adsorption of uranium (VI) from aqueous solutions : Kinetic and equilibrium profiles. *Chemical Engineering Journal* **273**, 390–400.

Anjum, M., Miandad, R., Waqas, M., Gehany, F. & Barakat, M. A. 2019 Remediation of wastewater using various nano-materials. *Arabian Journal of Chemistry* **12**, 4897–4919.

Anush, S. M., Chandan, H. R. & Vishalakshi, B. 2019 Synthesis and metal ion adsorption characteristics of graphene oxide incorporated chitosan Schiff base. *International Journal of Biological Macromolecules* **126**, 908–916.

Atkovska, K., Lisichkov, K., Ruseska, G. & Dimitrov, A. T. 2018 A Removal of heavy metal ions from wastewater using conventional and nanosorbents: A review. *Journal of Chemical Technology and Metallurgy* **53**, 202–219.

Ben-Ali, S., Jaouali, I., Souissi-Najar, S. & Ouederni, A. 2017 Characterization and adsorption capacity of raw pomegranate peel biosorbent for copper removal. *Journal of Cleaner Production* **142**, 3809–3821.

Berger, E., Haase, P., Kuemmerlen, M., Leps, M., Bernhard, R. & Sundermann, A. 2017 Water quality variables and pollution sources shaping stream macroinvertebrate communities. *Science Total Environment* **588**, 1–10.

Bhanjana, G., Dilbaghi, N., Kim, K. & Kumar, S. 2017 Carbon nanotubes as sorbent material for removal of cadmium. *Journal of Molecular Liquids* **242**, 966–970.

Brandes, R., Belosinschi, D., Brouillette, F. & Chabot, B. 2019 A new electrospun chitosan/phosphorylated nanocellulose biosorbent for the removal of cadmium ions from aqueous solutions. *Journal of Environmental Chemical Engineering* **7** (6), 103477.

Briffa, J., Sinagra, E. & Blundell, R. 2020 Heavy metal pollution in the environment and their toxicological effects on humans. *Heliyon* **6**(9), e04691. https://doi.org/10.1016/j.heliyon.2020.e04691.

Do Nascimento, J. H. O., Luz, R. F., Galvao, F. M. F., Melo, J. D. D., Oliveira, F. R., Ladchumananandasivam, R. & Zille, A. 2015 Extraction and characterization of cellulosic nanowhisker obtained from discarded cotton fibers. *Materials Today: Proceedings* **2**(1), 1–7.

Gaurav, B., Neeraj, D., Ki-Hyun, K. & Sandeep, K. 2017 Carbon nanotubes as sorbent material for removal of cadmium. *Journal of Molecular Liquids* **242**, 966–970.

Gopal Reddi, M. R., Gomathi, T., Saranya, M. & Sudha, P. N. 2017 Adsorption and kinetic studies on the removal of chromium and copper onto Chitosan-g-maliec anhydride-g-ethylene dimethacrylate. *International Journal of Biological Macromolecules* **104**, 1578–1585.

Haoyuan, J., Simiao, W. & Jizhi, Z. 2023 Preparation and modification of nanocellulose and its application to heavy metal adsorption: A review. *International Journal of Biological Macromolecules* **236**, 123916. https://doi.org/10.1016/j.ijbiomac.2023.123916.

Harini, K., Ramya, K. & Sukumar, M. 2018 Extraction of nano cellulose fibers from the banana peel and bract for production of acetyl and lauroyl cellulose. *Carbohydrate Polymers* **201**, 329–339.

He, C., Yang, Z., Ding, J., Chen, Y., Tong, X. & Li, Y. 2017 Effective removal of Cr(VI) from aqueous solution by 3-aminopropyltriethoxysilane-functionalized graphene oxide. *Colloids and Surfaces* **520**, 448–458.

Hokkanen, S., Bhatnagar, A. & Sillanpaa, M. 2016 A review on modification methods to cellulose-based adsorbents to improve adsorption capacity. *Water Research* **91**, 156–173.

Ibrahim, T. N. B. T., Othman, F. & Mahmood, N. Z. 2020 Baseline study of heavy metal pollution in a tropical river in a developing country. *Sains Malaysiana* **49**(4), 729–742.

Igberase, E., Ofomaja, A. & Osifo, P. O. 2019 Enhanced heavy metal ions adsorption by 4-aminobenzoic acid grafted on chitosan/epichlorohydrin composite: Kinetics, isotherms, thermodynamics and desorption studies. *International Journal of Biological Macromolecules* **123**, 664–676. https://doi.org/10.1016/j.ijbiomac.2018.11.082.

Jianhua, Q., Xue, T., Zhao, J., Bo, C., Modupe, S. A., Qi, H., Chengcheng, F., Yan, F., Xianlin, M. & Ying, Z. 2020 Multi-component adsorption of Pb(II), Cd(II) and Ni(II) onto microwavefunctionalized cellulose: Kinetics, isotherms, thermodynamics, mechanisms and application for electroplating wastewater purification. *Journal of Hazardous Materials* **387**, 121718. *Journal of Chemical Technology Metallargy*, Vol. 53(2), 202-219.

Kara, H. T., Anshebo, S. T. & Sabir, F. K. 2020 A novel modified cellulose nanomaterials (CNMs) for remediation of chromium (VI) ions from wastewater A novel modi fied cellulose nanomaterials (CNMs) for remediation of chromium (VI) ions from wastewater. *Materials Research Express* **7**(2020), 115008.

Kara, H. T., Anshebo, S. T. & Sabir, F. K. 2021a Adsorptive removal of Cd (II) ions from wastewater using maleic anhydride nanocellulose *Journal of Nanotechnology* **2021**, 15.

Kara, H. T., Anshebo, S. T., Sabir, F. K. & Workineh, G. A. 2021b Removal of methylene blue dye from wastewater using periodiated modified nanocellulose. *International Journal of Chemical Engineering* **2021**, 16.

Kim, J. H., Shim, B. S., Kim, H. S., Lee, Y. J., Min, S. K., Jang, D. & Kim, J. 2015 Review of nanocellulose for sustainable future materials. *International Journal of Precision Engineering and Manufacturing Green Technology* **2**(2), 197–213.

Maharana, M., Manna, M., Sardar, M. & Sen, S. 2020 *Heavy Metal Removal by Low-Cost Adsorbents*. Vol. *September* 2020, 245–272. https://doi.org/10.1007/978-3-030-47400-3-10.

Matsis, V. M. & Grigoropoulou, H. P. 2008 Kinetics and equilibrium of dissolved oxygen adsorption on activated carbon. *Chemical Engineering Science* **63**, 609–621.

Mohd Nor, F. N., Noor Azilah, M. K., Victor, F. K., Muhammad, S. M. M., Nurjahirah, J., Noor Aisyah, A. S., Norherdawati, K., Siti Aminah, M. N., Siti, H. J. K. K. O. and Wan Md, Z. W. Y. 2021 Nanocellulose: A bioadsorbent for chemical contaminant remediation. *RSC Advances* **11**, 7347–7368.

Mohib, U., Ruqia, N., Muslim, K., Waliullah, K., Mohib, S., Sahib, G. A. & Amir, Z. 2020 The effective removal of heavy metals from water by activated carbon adsorbents of Albizia lebbeck and Melia azedarach seed shells. *Soil and Water Research* **15**, 30–37.

Nguyen, K. M., Nguyen, B. Q., Nguyen, H. T. & Nguyen, H. T. H. 2019 Adsorption of arsenic and heavy metals from solutions by unmodified iron-ore sludge. *Applied Science* **9**, 619.

Rathnasekara, R. A. S. D., Botheju, W. S. M., Liyanage, J. A., Weragoda, S. K. & Kularathne, K. A. M. 2021 Risk assessment of trace element contamination in drinking water and agricultural soil : a study in selected chronic kidney disease of unknown etiology (CKDu) endemic areas in Sri Lanka. *Journal of Chemistry* **2021**, 1–10.

Shahnaz, T., Sharma, V., Subbiah, S. & Narayanasamy, S. 2020 Multivariate optimisation of Cr (VI), Co (III) and Cu (II) adsorption onto nanobentonite incorporated nanocellulose/chitosan aerogel using response surface methodology. *Journal of Water Processing Engineering* **36**, 101283.

Sharma, P., Tripathi, S. & Chandra, R. 2021 Highly efficient phytoremediation potential of metal and metalloids from the pulp paper industry waste employing Eclipta alba (L) and Alternanthera philoxeroide (L): Biosorption and pollution reduction. *Bioresource Technology* **319**, 124147. https://doi.org/10.1016/j.biortech.2020.124147.

Sun, J., Chen, Y., Yu, H., Yan, L., Du, B. & Pei, Z. 2018 Removal of Cu^{2+}, Cd^{2+} and Pb^{2+} from aqueous solutions by magnetic alginate microsphere based on Fe_3O_4/MgAl-layered double hydroxide. *Journal of Colloid and Interface Science* **532**, 474–484.

Tana, K. B., Reza, A. K., Abdullah, A. Z., Horri, B. A. & Salamatinia, B. 2018 Development of self-assembled nanocrystalline cellulose as a promising practical adsorbent for methylene blue removal. *Carbohydrate Polymers* **199**, 92–101.

Thommes, M., Kaneko, K., Neimark, A. V., Olivier, J. P., Rodriguez-Reinoso, F., Rouquerol, J. & Sing, K. S. W. 2015 Physisorption of gases, with special reference to the evaluation of surface area and pore size distribution (IUPAC Technical Report). *Pure Applied Chemistry* **87**, 1051–1069.

Tsade, H., Murthy, H. C. A. & Muniswamy, D. 2020 Bio-sorbents from agricultural wastes for eradication of heavy metals: A review. *Journal of Materials and Environmental Science* **11**(10), 1719–1735.

Tsade, H., Anshebo, S. T. & Sabir, F. K. 2021 Preparation and characterization of functionalized cellulose nanomaterials (CNMs) for Pb (II) ions removal from wastewater. *Journal of Chemistry* **2021**, 18.

Tshikovhi, A., Mishra, S. B. & Mishra, A. K. 2020 Nanocellulose-based composites for the removal of contaminants from wastewater. *International Journal of Biological Macromolecules* **152**, 616–632.

Unuabonah, E. I., Adebowale, K. O. & Olu-Owolabi, B. I. 2007 Kinetic and thermodynamic studies of the adsorption of lead (II) ions onto phosphate-modified kaolinite clay. *Journal of Hazardous Materials* **144**, 386–395.

Xu, Q., Wang, Y., Jin, L., Wang, Y. & Qin, M. 2017 Modified cellulose membrane with good durability for effective oil-in- water emulsion treatment. *Journal of Hazardious Matererials* **339**, 91–99.

Yang, X., Han, F., Xu, C., Jiang, S., Huang, L., Liu, L. & Xia, Z. 2017 Effects of preparation methods on the morphology and properties of nanocellulose (NC) extracted from corn husk. *Industrial Crops and Products* **109**, 241–247.

Yeit, H. T., Siti, N. A. & Kah, C. H. 2020 Sustainable approach to the synthesis of cellulose membrane from oil palm empty fruit bunch for dye wastewater treatment. *Journal of Water Process Engineering* **34**, 101182.

Zhou, Y., Jin, Q., Hu, X., Zhang, Q. & Ma, T. 2012 Heavy metal ions and organic dyes removal from water by cellulose modified with maleic anhydride. *Journal of Material Science* **47**, 5019–5029.

First received 6 October 2023; accepted in revised form 8 March 2024. Available online 9 April 2024